Particle Beam Waist Location in Plasma Wakefield Acceleration

Adrian Down*
Department of Physics, University of California, Los Angeles†
(Dated: September 27, 2006)

The role of beam waist location in interactions between a plasma and a particle beam is not yet fully understood. Nonlinear effects within the plasma make an analysis of such interactions difficult. I present five simulations in which I vary the waist location of a beam of ultra-relativistic electrons propagating through one meter of self-ionized lithium plasma. The simulation parameters are chosen to model the recent experiment 167 at the Stanford Linear Accelerator, relevant to the design of future plasma wakefield accelerating afterburners. I find that beams focused near the point of entry into the plasma propagate further into the plasma and accelerates witness particles to a greater maximum energy before disintegrating. These results could indicate that ion channel formation is dependent on the drive beam waist location and that the plasma accelerating medium can have an observable effect on the focusing of the drive beam.

Contents

INTRODUCTION

Experiments using high energy particle accelerators have led to discoveries about the structure of matter, astrophysical processes, and the early history of the universe [1]. Future colliders that accelerate particles to higher energies could provide insight into the nature of mass and the unification of the fundamental forces of nature [2]. Constructing higher energy particle accelerators could contribute to research in many branches of physics. Particles accelerated to lower energy are useful for other purposes and are an important source of radiation for research and medical devices.

In conventional colliders, particles are accelerated using electric fields produced by microwave radiation. These fields travel synchronously with the particles to be accelerated [2]. The energy of the accelerated particles is a function of the strength of the accelerating field and the distance over which the field acts.

The fields that can be achieved by this radio frequency (RF) technology are fundamentally limited by the structural integrity of the collider apparatus. RF accelerating fields are generated in metal devices called slow wave cavities. Increasing the field in these cavities far beyond levels employed in current high energy colliders leads to electrical breakdown within the cavities and ionization of the materials with which the cavities are constructed [1].

Because the fields achievable using RF technology are limited, the energies that can be obtained with this technology have thus far been increased by increasing the distance over which the accelerating field acts. The highest

energy RF collider is currently the Large Hadron Collider, under construction at CERN [2] and scheduled to be completed in 2007. At this enormous facility, protons will circle a loop 8.7 km in radius before colliding with seven TeV of energy. Continuing to advance the energy frontier of RF accelerators by increasing the size of the devices faces shortfalls of funding and resources. Plans for a Superconducting Super Collider that would be 28 km in diameter and cost 8 billion dollars to construct were cancelled by congress in 1993, and a proposed linear collider 30 km in length has yet to receive funding [3].

New techniques for accelerating particles using plasmas could soon produce smaller, less expensive colliders and extend the energy frontier beyond that set by current RF technology. In a plasma accelerator, an ionized gas of electrons and positive ions is used to generate accelerating fields. The fields that can be achieved in plasmas are over a thousand times greater than those that can be achieved in RF accelerators [3] and are not limited by the breakdown of the apparatus [1].

Energies achievable using plasma acceleration have been increasing by an order of magnitude every five years for the past decade [2], as shown in figure 1. Due to larger accelerating fields, plasma acceleration devices are generally much smaller than comparable RF accelerators. Smaller accelerators require smaller beam sizes. Fortunately, a plasma can act as a focusing lense in certain situations.

While plasma particle accelerators may replace RF technology at the energy frontier, compact lower energy plasma accelerators could be used in the fields of materials science, structural biology, nuclear medicine, fusion research, food sterilization, and medical therapy. Plasma

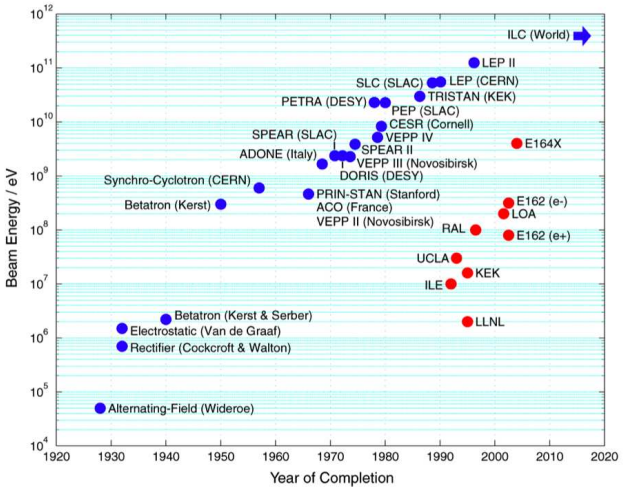

FIG. 1: The Livingston plot showing the energy of RF (blue) and plasma (red) acceleration techniques. Energies obtainable in plasma acceleration experiments have risen rapidly over the last decade and may soon surpass energies achievable with RF technology [4].

accelerators could also provide new sources of x-rays and gamma rays. Observing the behavior of charged particles in plasmas provides an opportunity to study the fields produced in this unique ionized environment and may contribute to the understanding of naturally occurring plasmas in astrophysical objects [1].

Plasma wakefield acceleration (PWFA) is a particular technique that shows promise for producing plasma accelerators at the energy frontier [4]. In PWFA schemes, a beam of ultra-relativistic[1] ($\gamma \gg 10^3$) particles is injected into a plasma. The behavior of the particles during acceleration and the maximum achievable energy is sensitive to the properties of the plasma and particle beam that are used.

The point at which the particle beam is focused is one such parameter that effects the PWFA process. The impact of focusing distance on the interaction fo a plasma and particle beam is not yet fully understood. The fields generated by the propagation of the particle beam through the plasma are highly nonlinear [5], and so an analytical description of the situation is difficult. A better understanding of the role of beam focusing distance in PWFA situations could lead to improved understanding of the physics of beam propagation within a plasma. The effects of beam focusing distance are also important to other areas of plasma research, such as inertial confinement fusion [6].

The envelope of a beam in an optical systems generally focuses to a plane of minimum transverse spot size, known as the waist of the beam, and then expands in the transverse direction in a manner that is longitudinally symmetric [7], as shown in figure 5.

In this study, I present the results of computer simulations performed with the QuickPIC algorithm [8] in which I vary the location of the plane of the beam waist relative to the plane at which the particle beam first encounters the plasma. I adjust the waist location in 5 cm increments from 0 cm to 25 cm in simulations of a 42 GeV electron beam propagating through a plasma of ionized lithium.

I find that focusing the particle beam near the entrance of the beam into the plasma, with the beam waist positioned at 0 and 5 cm, results in a longer propagation distance of the particle beam and a higher maximum energy of the accelerated particles relative to beams focused more deeply in the plasma, such as a beam with 20 or 25 cm waist location. Although shallowly focused beams propagate a longer distance than those focused more deeply within the plasma, shallowly focused beams appear to be more susceptible to instabilities.

These simulations are directly relevant to the recent

[1] This and all other symbols used in the text are defined in table I.

experiment 167 at the Stanford Linear Accelerator Center (SLAC). In this experiment, the SLAC electron beam was passed through a meter of lithium vapor that became ionized upon impact of the electron beam. Some beam particles achieved spectacular energy gain, doubling energy from 42 GeV to over 80 GeV in a distance of one meter [9]. However, the experimental results show a spectrum of particles with energies extending far below those observable in computer simulations. This study of beam waist position in PWFA suggests that these particles are likely self-trapped during the acceleration process.

Based on these simulations, it appears that the minimum spot size of the beam in the E-167 simulations may not be as small as initially believed, which is contrary to the expectation that the plasma should act as a focusing device. These results may also challenge the assumption that the envelope of the beam in the plasma evolves as if the beam were propagating in vacuum.

BACKGROUND

Plasma wakefield acceleration

Basic wakefield formation

In most plasma acceleration schemes, a high energy beam, called the drive beam, consisting either of laser photons or charged particles is shot into a plasma. Plasma wakefield acceleration (PWFA) refers to the case in which the drive beam is composed of ultra-relativistic charged particles ($\gamma \gg 10^3$), usually electrons [10].

The plasma into which the drive beam is shot is initially electrically neutral. Upon impact from the drive beam, plasma electrons in the vicinity of the beam are expelled to preserve the charge neutrality of the plasma [10]. The positive plasma ions are much more massive than the negative plasma ions and are approximately unaffected by the incoming drive beam. The plasma electrons beyond a few skin depths from the beam path are unaffected by the presence of the beam [5].

Parameter	Symbol
Electron mass	m
Speed of light in vacuum	c
Beam (plasma) number density	n_b (n_p)
Electron plasma frequency	$\omega_p = \left(n_p e^2/\epsilon_0 m\right)^{1/2}$
Collisionless plasma skin depth	c/ω_p
Electron plasma wave number	$k_p = \omega_p/c = 2\pi/\lambda_p$
Total number of beam particles	N
Longitudinal r.m.s. beam spot size	σ_z
Transverse r.m.s. beam spot size	σ_r
Beam normalized velocity	$\beta = v_b/c$
Beam lorentz factor	$\gamma = (1-\beta^2)^{-1/2}$
Beam betatron oscillation frequency	$\omega_b = \omega_p/\left(2\gamma\right)^{1/2}$
Beam emittance	ϵ
Beam normalized emittance	$\epsilon_N = \gamma\epsilon$

TABLE I: Definition of symbols used in text [10]

The behavior of the beam in the plasma depends on the relative densities of the plasma and the incoming beam. If $n_b < n_p$ and $k_p\sigma_r \ll 1$, meaning that the transverse beam spot size is much less than the plasma wavelength, the beam is pinched by its own magnetic field [10]. Otherwise, if $n_b > n_p$, called the underdense regime, the plasma electrons are expelled to a distance of several collisionless skin depths from the beam axis [5].

The positive ion channel left in the wake of the drive beam exerts an attractive Coulomb force on the expelled plasma electrons. The electrons return to the beam axis in about a plasma period, or in the frame of reference of the moving beam, one plasma wavelength behind the drive beam [5]. Due to their momentum, the electrons overshoot the beam axis and continue to oscillate in the transverse direction.

If $n_b \gg n_p$ and $k_p\sigma_r \ll 1$, nearly all plasma electrons are expelled by the drive beam. The transverse beam dynamics are simplified somewhat in this 'blowout regime', as the radial focusing force produced by the positive ion column is linear. In this case, the ion channel can be treated as a uniform cylinder of positive charge, and the field within the ion channel can be obtained from Gauss's law,

$$E_r = -\frac{1}{2}\frac{n_p e}{\epsilon_0} r \tag{1}$$

As the particle beam propagates forward, these oscillating electrons set up a wakefield consisting of a series of regions of positive charge, known as 'buckets', each followed by a dense region of negative charge, as shown in figure 2. High electric fields can develop in the region within the positive ion channel at the rear of each bucket immediately preceding the region of dense negative charge.

Linear theory predicts that the peak accelerating field that can be obtained using the PWFA method is [10],

$$(eE)_{\text{linear}} = 240(\text{MeV/m}) \left[\frac{N}{4\times 10^{10}}\right] \left[\frac{0.6\text{ mm}}{\sigma_z}\right]^2 \tag{2}$$

Although the underdense regime, $n_b > n_p$, is desirable for particle acceleration, linear theory is no longer valid in this regime. Due to nonlinearities, the underdense regime must be studied with particle-in-cell (PIC) computer simulations. One important linear theory result, namely that $(eE) \propto \sigma_z^{-2}$, appears to remain valid when the underdense plasma condition is satisfied [10].

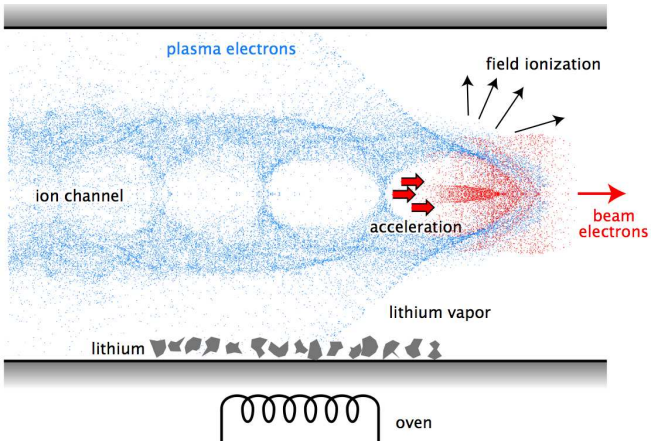

FIG. 2: Wakefield formation. A drive pulse expels plasma electrons, creating a column of positive ions. Plasma electron oscillations create 'buckets' containing large electric fields that can be used for particle acceleration [4].

Acceleration gradients achieved in the underdense regime can be greater than those predicted by linear theory. As shorter drive beam bunch lengths become possible, acceleration gradients of more than 40 GeV/m can can be realized [10]. In comparison, the SLAC accelerates particles to approximately 40 GeV of energy over a distance of about 3.2 km.

Achieving high energies with plasma accelerators relies on the ability to inject charged particles into the region of maximum accelerating gradient at the rear of the first bucket. A pulse, called the witness beam, is launched behind the drive beam. The timing is such that the witness beam experiences the maximum accelerating gradient once the wakefield is formed by the drive beam. As the drive beam propagates through the plasma, the particles in the witness beam are influenced by the accelerating field and gain energy.

Because the drive beam is ultra-relativistic, the witness beam must also be ultra-relativistic before injection. The witness beam travels at nearly the speed of light, and so most energy gained from acceleration is due to change in momentum rather than change in speed. Thus the witness beam does not outrun the drive pulse as acceleration proceeds. In effect, the plasma acts as a transformer: the energy of the drive beam is transferred to the plasma in the formation of the wake, which is in turn transferred to the witness beam as it is accelerated.

Betatron oscillation

The focusing force exerted by the ion channel can cause the electrons of the drive beam to oscillate about the axis of the beam. In the blowout regime, the focusing force exerted by the ion channel given by equation (1) can be recast in terms of the plasma wave number [11],

$$F_r = eE_r = -\frac{1}{2}\frac{n_p e^2}{\epsilon_0} r = -\frac{1}{2} mc^2 k_p^2 r \tag{3}$$

The relativistic equation of motion for a single beam electron is thus,

$$F_r = \frac{dp_r}{dt} = \frac{d}{dt}\left(\gamma m v_r\right) \tag{4}$$

Because the beam is ultra-relativistic, the relation $z = ct$ can be used to rephrase (4) in terms of the longitudinal location z,

$$\frac{d\left(\gamma m \frac{dr}{d(z/c)}\right)}{d(z/c)} = -\frac{1}{2} mc^2 k_p^2 r$$
$$\frac{d}{dz}\left(\gamma \frac{dr}{dz}\right) + \frac{1}{2} k_p^2 r = 0 \tag{5}$$

(5) can be written as the equation of motion for a simple harmonic oscillator with the definition[2] $k_\beta = k_p/(2\gamma)^{1/2}$,

$$\frac{d}{dz}\left(\gamma \frac{dr}{dz}\right) + \gamma k_\beta^2 r = 0 \tag{6}$$

The transverse oscillation of beam electrons described by (6) is known as betatron oscillation. The frequency of this oscillation $\omega_\beta = \omega_p/(2\gamma)^{1/2}$ is energy dependent, and thus particles in a non-monoenergetic beam can undergo betatron oscillation at varying frequencies. Interference of differing betatron frequencies can lead to scalloping in the beam shape, as shown in figure 17, which results as the wakefield acceleration process widens the energy distribution of the drive beam.

Betatron oscillation of individual particles within a beam can cause the envelope of the beam to oscillate. An equation describing the beam envelope can be obtained by summing the oscillations of all individual electrons. The result is [10],

$$\sigma_r''(z) + \left(k_\beta^2 - \frac{\epsilon_N^2}{\gamma^2 \sigma_r^4(z)}\right) \sigma_r(z) = 0 \tag{7}$$

The frequency of envelope oscillation is twice that of the oscillation frequency of individual particles. This fact is a simple consequence of the geometry of the beam, as shown in figure 3.

It is possible to eliminate the oscillation of the beam envelope by setting $\sigma_r''(z) = 0$ in (7). The initial radius that satisfies this condition is known as the matched radius, $r_{bm} = (\epsilon_N/\gamma k_p)^{1/2}$ [10]. If the radius of the beam at the entry to the plasma is any other than the matched radius, the envelope of the beam will undergo betatron oscillations.

[2] The normalized emittance ϵ_N which appears in (6), is discussed in the later section "Phase space analysis of beam optics."

Ion channel formation in self-ionized regime

A particle beam with sufficiently high current density can simultaneously ionize a neutral gas into a plasma and create the wakefield structure. The radial electric field is that which governs the formation of the ion channel. The maximum radial electric field is proportional to the current density of the drive beam [12],

$$E_{r,\max} \propto \frac{N}{\sigma_r \sigma_z} \tag{8}$$

Thus short beams with small spot size are most effective at producing self-ionized plasma.

As a first approximation, ionization of the plasma medium occurs when the electric field produced by the drive beam exceeds the electric force binding the plasma electrons to the positive ions in the unionized state. The ionization front is defined as the plane in which the entire transverse profile of the drive beam lies within the ion column, as shown in figure 4.

The head of the drive pulse in the self-ionization process is ahead of the ion channel and thus does not experience the focusing force of the positive ions. The head of the beam expands, which by (8), causes the maximum radial electric field to decrease. As the field decreases, the ionization front moves further towards the rear of the drive pulse [12]. This process, known as head erosion, reduces the effective accelerating field within the wake and can lead to the eventual disintegration of the beam.

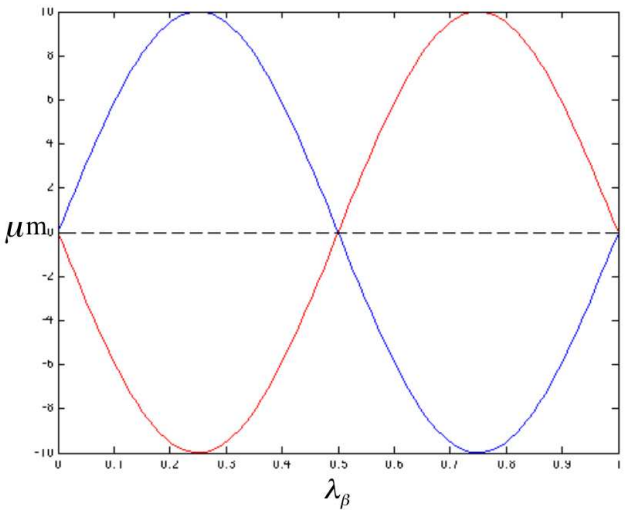

FIG. 3: Two particles at the same energy undergo a single betatron oscillation. Because the particles are symmetrically located, the envelope of the beam experiences two complete oscillations.

Plasma focusing

The rate at which particles are collided in an accelerator is as important to the usefulness of the apparatus as the total collision energy. Fewer particles are accelerated to the highest energies in a plasma accelerator relative to a comparable RF accelerator. To be competitive with RF accelerators at the energy frontier, plasma devices must achieve a large number of collisions of the highest energy particles.

One technique to ensure that an adequate number of high energy collisions occur is to reduce the transverse spot size of the beam while holding the beam density constant, thereby increasing the probability of collision and preserving the overall event rate. For plasma particle accelerators to be competitive at high energies using existing techniques, the particle drive beams must be focused dow to a few tens of nanometers [3].

The plasma accelerating medium itself can act as a focusing lens, contributing to the desired reduction in spot

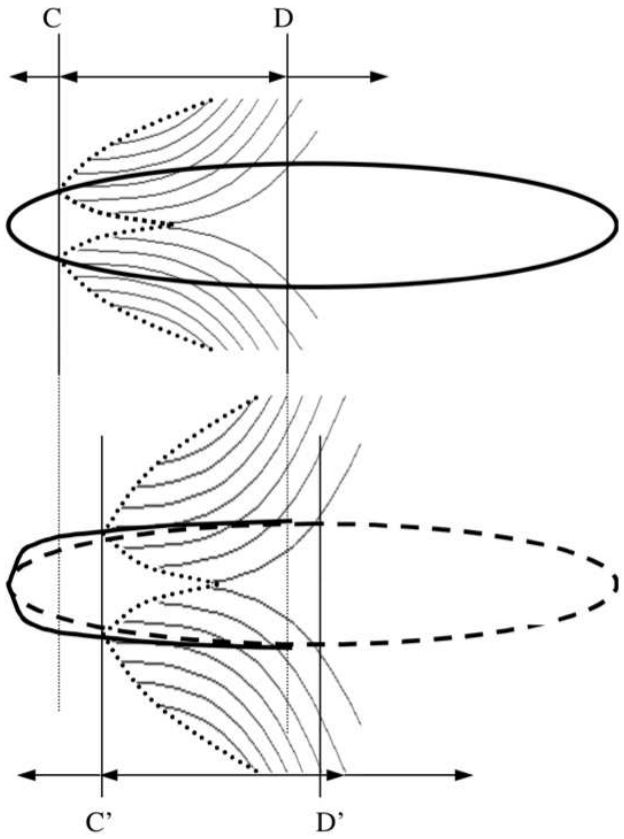

FIG. 4: Self-ionization process, in which the plasma medium is ionized and the wakefield is created by a single drive pulse. The ionization front, labeled D above, is the plane in which the entire transverse profile of the drive beam lies within the ion column. The portion of the beam ahead of the ion front is eroded, and the ionization front moves towards the rear of the drive pulse.

size. The radial focusing force due to the ion channel in the blowout regime, as given by (3), is linearly proportional to the distance from the beam axis. This focusing mechanism can reduce beam spot size by a factor of about two to four using PWFA techniques [3].

Plasma afterburners

PWFA technologies can be used to extend the energy range of existing RF accelerators. Devices called 'plasma afterburners' are currently being developed that may, in the future, increase the energies of existing colliders by a factor of two or more.

Afterburners consist of a tube of plasma placed in the beam line of an RF accelerator near the collision point. Particles accelerated using RF fields serve as the drive pulse for the plasma afterburner. The particle bunch produced by the collider ideally consists of two microbunches, each approximately 100 femtoseconds in length, separated by about 100 femtoseconds. The first bunch ionizes the plasma and excites the wake, and the second bunch, containing about one third as much charge as the drive pulse, is trapped in the wake and accelerated.

Current predictions imagine plasma columns about 10 meters long, one on each side of the collision point of the collider. Due to the energy spreading that occurs in the plasma, it would be necessary to focus the beam to tighter spot sizes to increase the collision rate of the collider. Fortunately, this could be accomplished with plasma lenses placed immediately at the exit of each afterburner. Due to the different dynamics of wakefield formation by positive drive particles, the positron beam afterburner would have a hollow channel.

Present difficulties

Radiation damping A beam undergoing betatron oscillations loses energy due to radiation resulting from the acceleration of the beam particles. This energy loss reduces the amount of energy available for acceleration. Betatron oscillation is essentially a simple harmonic oscillation process, and thus the magnitude of the acceleration experienced by the charge depends strongly on the initial displacement of the charge from the axis of the beam when the beam enters the plasma [13]. The resulting radiative losses could lead to an undesirable spread in energy of the accelerated particles.

Although the energy lost to radiation is undesirable for acceleration purposes, the resulting photons can be a useful source of radiation for optical purposes [4].

Hosing instability The hosing instability refers to the tendency of small perturbations of a beam propagating through a plasma to be amplified. The effect is due to a nonlinear coupling of the beam electrons to the plasma electrons at the edge of the beam [14]. The nonlinear growth of transverse perturbations can eventually lead to the breakup of the beam.

Experimental results and simulations show that the effect of the hosing instability is not as severe as initially thought [4]. Imperfections in the beam, such as asymmetries and longitudinal density gradients within the beam, tend to suppress the growth of hosing instabilities. However, the hosing instability can become significant when propagating PWFA beams distances on the order of a meter or more through a plasma.

Trapped particles As a particle beam travels through a plasma, the resulting wakefield can can trap plasma particles. Trapping can result from multiple ionization of the plasma medium.

Since particles can become trapped at any point and are rarely trapped in the region of highest field gradient, the energy gain of the trapped particles is usually much less than that of the witness bunch. Hence these trapped particles are doubly problematic in that they appear as low energy noise in energy diagnostics and also extract energy from the wakefield that could otherwise go to acceleration of the witness bunch.

Emittance Twiss parameters

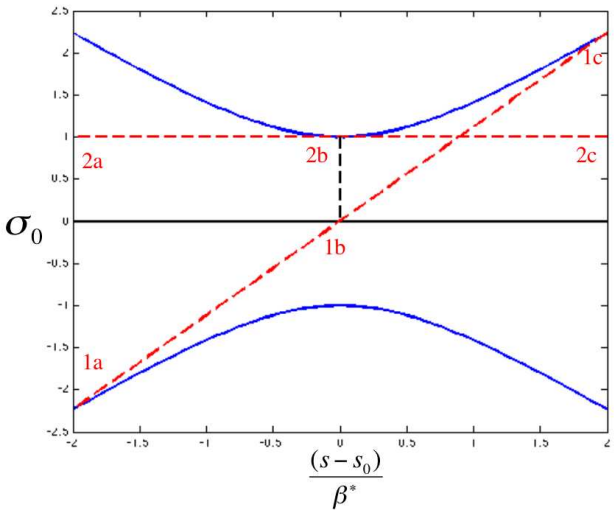

FIG. 5: One-dimensional profile of beam envelope (blue) near waist (vertical dashed line). Red dashed lines track motion of two particles as beam propagates in the longitudinal direction. The phase space evolution of these particles is shown in figure 6.

Beam Focusing

Often it is desirable to reduce the spot size of a beam used in an optical system. This can be accomplished by imparting the beam particles farthest from the beam axis with transverse momentum towards the beam axis. If the beam particles receive no further perturbations, the beam envelope contracts to minimum spot size. The location of the plane at which this minimum occurs is known as the beam waist. The beam envelope expands symmetrically on the opposite side of the beam waist [7], as shown in figure 5.

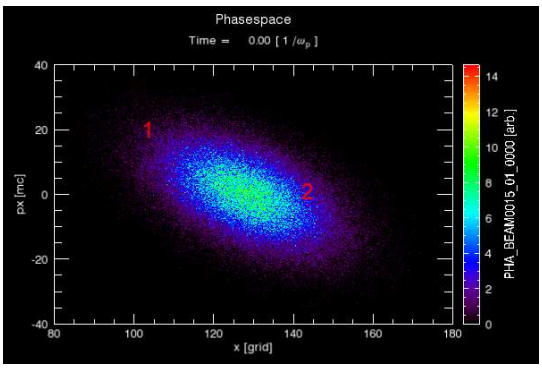

(a)Converging beam approaching waist.

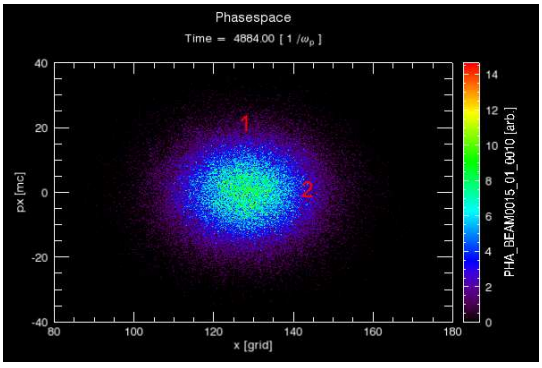

(b)Beam at waist.

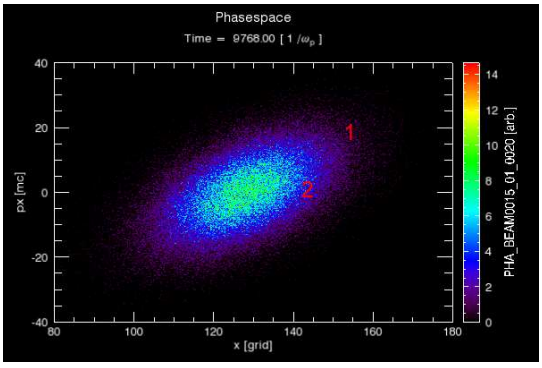

(c)Diverging beam located at point symmetric about waist in transverse direction.

FIG. 6: Phase space evolution in one spatial dimension of a typical optical beam near waist. Red numbers show location of two particles whose trajectories are plotted in figure 5.

In the case that the beam is not azimuthally symmetric, the waist location can vary for differing transverse direction. The beam envelope will evolve independently in the two planes formed by the transverse coordinate axes, respectively, and the beam axis.

Consider a single transverse dimension of a beam undergoing focusing. I call this arbitrary direction y in the discussion that follows. Beam particles farthest from the beam axis are given transverse momentum to reduce the spot size of the beam. Hence particles at large $-y$ receive momentum in the positive transverse direction, and particles at large $+y$ receive momentum in the negative transverse direction.

The behavior of a representative particle is shown in figure 5, labeled '1'. Assuming no forces act on the beam particles, the transverse momentum of particle 1 carries it through the beam axis. The particle continues past the beam axis. Similar behavior of other beam particles results in expansion of the beam envelope as the beam propagates past the plane of the waist.

Because of focusing imperfections, some beam particles off the beam axis receive no transverse momentum. These particles limit the minimum spot size of the beam. A representative particle is labeled as '2' in figure 5. As the beam propagates, such particles maintain constant transverse positions.

Phase space analysis

It is useful to analyze the focusing of such a beam in phase space. The phase space description leads to the definition of emittance and the Twiss parameters. The emittance is an important characterization of the angular spread of the beam, and the Twiss parameters can be used to specify the waist location of the beam.

The phase space evolution of a beam undergoing focusing, including the representative particles 1 and 2 referenced in figure 5, appears in figure 6. Because the beam is assumed to be propagating in free space, the momentum of any given beam particle is unchanged. Hence the vertical position of any point in the phase space diagram is fixed.

However, the transverse position of beam particles can change as the beam propagates. The change in transverse position is proportional to transverse momentum, which is represented on the vertical axis of the phase space plot. Hence the horizontal movement of a point in phase space is in proportion to its constant vertical position.

As stated above, particles initially with most negative position begin with most positive momentum, and vice versa for particles at positive transverse position. The anti-correlation of position and momentum results in an ellipse in phase space that slopes from the upper left to the lower right, as shown in figure 6.

The horizontal axis of the ellipse corresponds to 0 transverse momentum. Hence the particles with no transverse momentum, such as particle 2, that determine the minimum spot size also determine the constant equatorial width of the phase space ellipse.

I consider a beam undergoing focusing prior to the beam reaching its waist. As the beam propagates, the spread in transverse position of the beam particles decreases. Particles with transverse momentum move towards the line $y = 0$ in phase space. Because the horizontal movement of points in phase space is in proportion to their vertical position, the phase space ellipse shears, with the portion in the upper half plane moving to the right and points below the horizontal axis moving to the left. At the waist, particles with maximal momentum magnitudes cross the beam axis, and so the vertical maxima of the ellipse are aligned so that the figure becomes circular.

As the beam propagates past the plane of the waist, the shearing of the phase space ellipse due to the initial transverse momentum of the beam particles continues. As particles with positive transverse momenta cross the beam axis and continue in the positive transverse direction, transverse position and momentum become positively correlated. The phase space diagram evolves to become an ellipse that is slanted from the lower left to the upper right, as shown in figure 6.

Emittance

Louisville's Theorem is a mathematical statement that the area in phase space of an ensemble of initial conditions of a non-dissipative system is constant. This theorem can be applied to a beam propagating in vacuum assuming the beam has a discrete envelope in phase space so that the concept of area is well defined. In this case, it is meaningful to define the emittance as a measure of the constant area of the phase space ellipse,

$$\epsilon = \frac{\text{area in phase space}}{\pi} \tag{9}$$

In the phase space plot, transverse position is measured in units of length, whereas momentum is usually written using normalized units so as to be effectively unitless. The unitless momentum can be assigned a unit of radians, so that emittance is often expressed in units of length · radians.

The emittance is a measure of the initial transverse momenta present in a beam. With knowledge of the distance over which the beam is propagated, the emittance can give information about the spot size of the beam. Alternatively, emittance can be interpreted independently of propagation distance as a measure of the angular spread of the beam. The normalized emittance $\epsilon_N = \gamma\epsilon$ takes into account the energy of the beam.

A transverse profile in phase space of physical particle beam is not bounded by a discrete beam envelope. In this case, the interpretation of ϵ as the phase space area spanned by all of the beam particles is no longer exact. However, the emittance can still be defined in this case to represent an average beam size in phase space,

$$\epsilon = \sigma_r \cdot \frac{v_T}{c} \tag{10}$$

where σ_r is the transverse r.m.s. beam spot size at the waist and v_T is the r.m.s. transverse velocity.

Twiss parameters

I return now to the discussion of a theoretical beam with discrete phase space envelope. Since the phase space ellipse of the beam is symmetric and has constant area, it can be uniquely characterized by three parameters [7]. The first of these parameters is the emittance. The other two parameters describe the shape of the phase space ellipse and are functions of the beam propagation distance z. These two functions are the Twiss parameters.

The amplitude function $\beta(z)$ is defined to describe the point on the ellipse with maximal transverse displacement,

$$y_{\max} = \sqrt{\epsilon\beta(z)} \tag{11}$$

The unit of radians is dropped from ϵ in (11), and so $\beta(z)$ is commonly expressed in units of length.

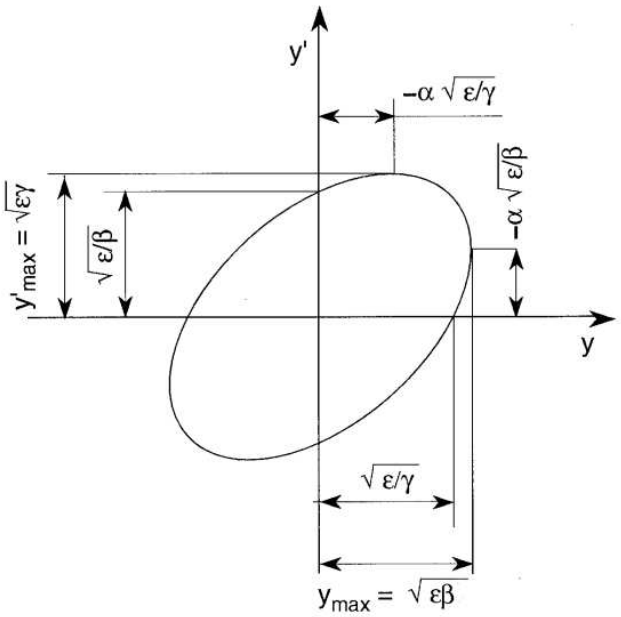

FIG. 7: Geometrical definition of emittance and Twiss parameters on a theoretical beam of definite envelope and constant density.

The other Twiss parameter $\alpha(z)$ is related to the point of maximal transverse momentum represented on the phase space ellipse,

$$y'_{\max} = \sqrt{\epsilon}\ \sqrt{\frac{1+\alpha^2}{\beta}} \tag{12}$$

Because ϵ and β carry the same units, modulo a dimensionless factor of radians, α is taken to be unitless.

(12) can be written more conveniently be defining the quantity[3] $\gamma \equiv (1+\alpha^2)/\beta$. With this definition, (12) becomes,

$$y'_{\max} = \sqrt{\epsilon\gamma} \tag{13}$$

Because the beam is assumed to be propagating in vacuum, the vertical position of each point of the phase space diagram is fixed. Hence γ is independent of the beam propagation distance. However, $\alpha(z)$ is dependent on the propagation distance through $\beta(z)$. This geometric interpretation of the Twiss parameters is shown in figure 7.

Relation of Twiss parameters to beam waist

In the simulations described in this paper, the drive beam is assumed to focus as if propagating in vacuum. This assumption is based on the fact that the plasma density is much less than the beam density. The focusing of the beam is modeled using the phase space analysis described above. The beam waist location is determined by specifying the values of the Twiss parameters at the plane at which the beam enters the plasma.

As noted above, the phase space plot of the beam becomes circular at the beam waist. From figure 7, the beam waist is thus characterized by the point at which $\alpha = 0$. The longitudinal position of the plane represented on a particular phase space diagram is related to the value of α at that longitudinal point [7],

$$z_{\text{waist}} - z = \frac{\alpha}{\gamma} \tag{14}$$

Hence $\alpha > 0$ implies that the beam is converging towards the waist, whereas $\alpha < 0$ implies that the beam has passed the waist and is diverging.

The value of $\beta(z)$ at the beam waist is a constant that parameterizes the minimum spot size of the beam. This value of β at the waist is written as β^*.

[3] The γ and β defined as Twiss parameters bear no relation to the relativistic factors $\gamma = (1-\beta^2)^{-1/2}$.

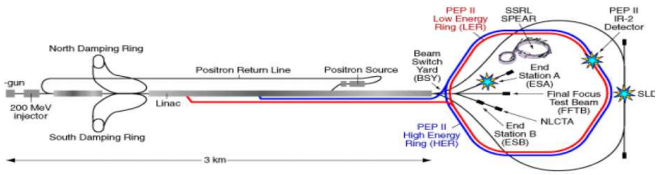

FIG. 8: Schematic diagram of the Stanford Linear Accelerator. The E-167 experiments are carried out in the Final Focus Test Beam (FFTB) facility.

METHODS

E-167 experiment

The E-167 experiments are a series of tests of technology to be used in future plasma afterburners. These tests began in 2005 at the Stanford Linear Accelerator Center (SLAC), and are currently in operation. Complete data from the experiments is forthcoming; however, preliminary results have already demonstrated energy doubling of some particles in the 42 GeV drive beam over a distance of 1 meter.

Apparatus

The E-167 experiments are being carried out at the Final Focus Test Beam (FFTB) facility at SLAC. This recently completed facility has the potential to create electron bunches with a minimum length of about 12 μm. These unprecedentedly short electron bunches can lead to higher radial electric fields in PWFA experiments, as predicted by (8). More precise control over the bunch length also allows the current profile of the drive and witness beams to be shaped so as to maximize the acceleration gradient experienced by the witness bunch [4].

Full details of the E-167 experimental apparatus are presented in [4]. A schematic diagram of the experimental apparatus is shown in figure 8. I summarize here some relevant aspects of the experiment.

The 42 GeV SLAC electron beam is passed through a tube containing 1 meter of lithium vapor. Lithium is chosen because the large ionization potential of the second bound electron of the lithium atom prevents significant secondary ionization from occurring when the drive beam is passed through the lithium vapor. Multiple ionization can lead to uncertainty in the electron density in the plasma and undesirable trapping of plasma electrons [15], as described above.

The lithium is initially electrically neutral and is vaporized by heating pellets of solid lithium. The lithium vapor becomes self-ionized upon impact with the SLAC electron beam. This drive beam simultaneously ionizes the lithium vapor and excites a wakefield structure.

The lithium vapor is bounded on each end by a helium

buffer gas, and the density of the plasma created from the lithium vapor can be controlled by adjusting the vapor density in the tube, a process which is precise and highly stable [4]. The stability of the vapor system implies that effects observed when the drive beam is passed through the plasma are likely due to properties of the drive beam itself and not due to the initial condition of the lithium plasma [15].

Diagnostics

The bunches used in the E-167 experiments are shorter than those used in past experiments. New data collection techniques are being developed that operate at the small time scales necessitated by short drive bunches.

The energy of the beam before entering the plasma is inferred from radiation emitted when the drive beam is deflected using chicane magnets. The synchrotron radiation resulting upon deflection is imaged on florescent Ce:YAG crystals. The amount of deflection experienced by beam particles, and hence the amount of emitted radiation, is proportional to the energy of the particles. Thus the observed radiation spectrum provides an unambiguous measurement of the energy profile of the beam [4].

Measurement of the bunch length is particularly difficult due to the short bunch lengths used in the E-167 experiment. Traditional measurement techniques cannot be used with high precision. Instead, beam particles are passed through a conducting foil, and the resulting coherent transition radiation is used as a measure of the longitudinal profile of the beam. A complete description of the method can be found in [16].

After emerging from the plasma, the beam is passed through an imaging spectrometer and the resulting spectrum is passed through a Cherenkov radiator. The emitted Cherenkov radiation is imaged on a piece of silica aerogel. As with the measurement of the initial beam energy, the radiation spectrum is interpreted as a measurement of the beam energy profile.

The energy profile observed after the beam has passed through the plasma can be calibrated against the initial beam energy by running the experimental apparatus with no lithium vapor. For calibration, the lithium vapor in the beam line can be exchanged for a vacuum in a matter of seconds [4].

Results

The E-167 experiments demonstrate the possibility of achieving unprecedented acceleration gradients. A small number of particles of the 42 GeV SLAC drive beam can double in energy to over 80 GeV in a distance of 1 m.

The energy spectra observed after the drive beam passes through the lithium plasma demonstrates unexpected behavior at low energy, however. As shown in figure 9, there is a tail of particles extending to very low energies. This monotonic tail of low energy particles is not reproduced by simulations, as shown in figure 21.

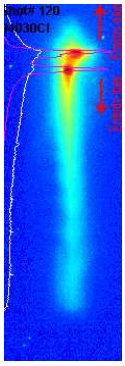

FIG. 9: Beam energy spectrum observed in E-167 experiment, as inferred from Cherenkov radiation upon deflection of beam. Energy is proportional to vertical position, with higher energies at greater vertical position. Vertical scale is not linear. The highest energy particles doubled in energy to over 80 GeV. The lowest energy particles form a monotonic tail that is not reproducible in simulations.

An explanation of the observed low energy spectrum could provide insight into the physical processes operative in PWFA. Studying these low energy particles could also help to improve simulations if there are effects that are not currently modeled correctly.

Simulations presented in this paper are not able to reproduce the observed spectrum of low energy particles by varying the beam waist position. Results of this study indicate that the tail of low energy particles shown in figure 9 is likely due to trapping of plasma electrons.

QuickPIC simulation algorithm

Introduction

Effective models of plasma based accelerators must simulate the evolution of the drive beam, the generation and evolution of the wake, and the acceleration of the witness bunch. Due to nonlinear effects, these tasks require particle based models. The particle-in-cell (PIC) algorithm is one such model that has shown good agreement with experimental results [8].

However, the full PIC model is too computationally intensive for large simulations. The simulations presented in this paper would take over 10^5 computer hours each if run using the full PIC model.

The QuickPIC algorithm reduces the necessary computational time by taking advantage of the different time scales of the evolution of the driver and the trailing beam. The drive beam evolves much slower than the wakefield structure, and so the QuickPIC algorithm operates on

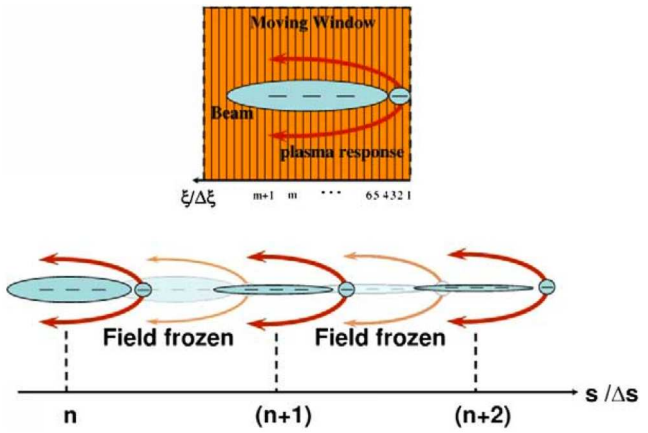

FIG. 10: Cartoon of quasi-static timescale separation in QuickPIC algorithm. The drive beam evolves more slowly than the wakefield structure. In the quasi-static approximation, the fields associated with the drive beam are held fixed as the beam is propagated over a distance Δs, whereas the wakefield structure is updated on a smaller timescale $\Delta\xi$.

a quasi-static model in which the drive beam is held constant over a specified distance while the wakefield is evolved at intermediate steps.

Quasi-static PIC equations

In PIC simulations, particles are located on a spatial grid. The charge and current densities calculated at grid points are used to advance the fields calculated from Maxwell's equations. The fields are used to advance the position and velocity of the particles using relativistic equations of motion.

The QuickPIC simulation algorithm begins with Maxwell's equations in the Lorentz gauge (in CGS units),

$$\left(\frac{1}{c^2}\frac{\partial}{\partial t^2} - \nabla^2\right)\phi(x,y,z,t) = 4\pi\rho(x,y,z,t) \tag{15}$$

$$\left(\frac{1}{c^2}\frac{\partial}{\partial t^2} - \nabla^2\right)\mathbf{A}(x,y,z,t) = \frac{4\pi}{c}\mathbf{J}(x,y,z,t) \tag{16}$$

where ϕ is related to the electric potential V, expressed in SI units, by $\phi = 4\pi\epsilon_0 V$.

The motion of plasma particles is determined from the Lorentz force equation,

$$\frac{d\mathbf{P}}{dt} = q\left(\mathbf{E} + \boldsymbol{\beta}\times\mathbf{B}\right) \tag{17}$$

where $\boldsymbol{\beta} = \frac{\mathbf{v}}{c}$.

It is convenient to transform to coordinates that reflect the different scales of the evolution of the drive beam and the wakefield structure,

$$s = z \qquad \xi = ct - z \tag{18}$$

with the accompanying Jacobians,

$$\frac{\partial}{\partial z} = -\frac{\partial}{\partial\xi} \qquad \frac{\partial}{c\,\partial t} = \frac{\partial}{\partial\xi} \tag{19}$$

ξ acts as a fast time scale associated with the driver and the development of wake. s acts as a slow time scale associated with the evolution of shape of the driver.

In these transformed coordinates, the quasi-static approximation is,

$$\frac{\partial}{\partial s} \ll \frac{\partial}{\partial\xi} \tag{20}$$

In this approximation, the wakefield is "frozen" as the drive beam is propagated over a number of small time steps $\Delta\xi$. The drive beam is updated on the slower time scale Δs. A cartoon schematic of how this approximation is used by the QuickPIC algorithm is shown in figure 10.

Beam evolution

The drive beam evolves on the time scale Δs, and so it will be convenient to write the equations governing the evolution of the drive beam in terms of the parameter s. Beam particles are treated as being ultra-relativistic, so that the velocity of beam particles $\mathbf{v}_b$ is approximately equal to $c\hat{\mathbf{z}}$. Thus longitudinal position can alternatively be used as a measure of time,

$$\frac{ds}{dt} \approx c \Rightarrow \frac{d}{dt} \approx c\frac{d}{ds} \tag{21}$$

(15) and (16) govern the evolution of the wakefield structure. Using (21), the longitudinal dependence in these equations cancels, leaving,

$$\nabla_\perp^2\phi(x,y,s,\xi) = -4\pi\rho(x,y,s,\xi) \tag{22}$$

$$\nabla_\perp^2\mathbf{A}(x,y,s,\xi) = -\frac{4\pi}{c}\mathbf{J}(x,y,s,\xi) \tag{23}$$

The Lorentz gauge condition can be expressed in s,ξ coordinates using (19),

$$\boldsymbol{\nabla}_\perp\cdot\mathbf{A}_\perp(x,y,s,\xi) = -\frac{\partial}{\partial\xi}\psi(x,y,s,\xi) \tag{24}$$

where $\psi = \phi - A_z$.

(17) describes the evolution of the momenta of beam particles. Before evaluating this equation, it is useful to recast the fields in terms of the electromagnetic potentials,

$$\mathbf{E} = -\nabla\phi - \frac{\partial\mathbf{A}}{c\,\partial t} \qquad \mathbf{B} = \boldsymbol{\nabla}\times\mathbf{A} \tag{25}$$

Using (25) and (19), (17) becomes,

$$\frac{d\mathbf{P}_{b\perp}}{ds} = -\frac{q_b}{c}\nabla_\perp\psi \qquad \frac{d\mathbf{P}_{bz}}{ds} = \frac{q_b}{c}\frac{\partial\psi}{\partial\xi} \tag{26}$$

The evolution equations for the transverse positions of the beam particles can be obtained from the definition of the relativistic momentum,

$$\mathbf{P}_{b\perp} = \gamma mc\boldsymbol{\beta} \tag{27}$$

$\boldsymbol{\beta}$ is related to the position,

$$\boldsymbol{\beta} = \frac{\mathbf{v}}{c} = \frac{d\mathbf{x}}{c\,dt} = \frac{d\mathbf{x}}{ds} \tag{28}$$

Substituting (28) into (27)

$$\frac{d\mathbf{x}_{b\perp}}{ds} = \frac{\mathbf{P}_{b\perp}}{\gamma mc} \tag{29}$$

Plasma wakefield evolution

The wakefield structure evolves on the shorter timescale corresponding to ξ. Hence I recast the Lorentz force equation (17) in terms of ξ,

$$\frac{d\mathbf{P}_{p\perp}}{d\xi} = \frac{d\mathbf{P}_{p\perp}}{dt}\frac{dt}{ds}\frac{ds}{d\xi} \tag{30}$$

The necessary derivatives are,

$$\begin{aligned} \frac{d\xi}{ds} &= \frac{d}{ds}(ct - z) = \frac{d}{c\,dt}(c\,dt) - \frac{dz}{ds} \\ \Rightarrow \frac{d\xi}{ds} &= 1 - \frac{P_z}{\gamma mc} = 1 - \beta_z \end{aligned} \tag{31}$$

Substituting (31) into (30),

$$\frac{d\mathbf{P}_{p\perp}}{d\xi} = \frac{q_p}{c - v_{pz}}\left[\mathbf{E}_\perp + (\boldsymbol{\beta}_p \times \mathbf{B})_\perp\right] \tag{32}$$

The longitudinal momentum of plasma particles can be obtained from a constant of the motion [8],

$$\gamma_p - \frac{P_{p\perp}}{mc} = 1 - \frac{q_p\psi}{mc^2} \tag{33}$$

where γ_p is the relativistic factor of the plasma particle.

The equation describing the evolution of the position of the plasma particles is obtained from (28) and (31),

$$\begin{aligned} \frac{d\mathbf{x}_{p\perp}}{d\xi} &= \frac{d\mathbf{x}_{p\perp}}{ds}\frac{ds}{d\xi} \\ &= \frac{\boldsymbol{\beta}_{p\perp}}{1 - \beta_{pz}} \end{aligned} \tag{34}$$

(32) and (34) determine the trajectory of each plasma particle as it is swept over by the drive beam.

Deposition scheme

The deposition scheme refers to the method by which the charge and current densities, ρ and $\mathbf{J}$, are determined from the charge, position, and momentum of individual particles. The method begins with the discreet version of conservation of charge,

$$0 = \underbrace{\frac{\partial}{\partial t}\sum_i Q_i\delta\left(\mathbf{x} - \mathbf{x}_i(t)\right)}_{\frac{\partial\rho}{\partial t}} + \underbrace{\boldsymbol{\nabla}\cdot\sum_i Q_i\mathbf{v}_i(t)\delta\left(\mathbf{x} - \mathbf{x}_i(t)\right)}_{\boldsymbol{\nabla}\cdot\mathbf{J}} \tag{35}$$

The perpendicular and $\hat{\mathbf{z}}$ components in the δ functions can be separated. Integrating (35) over z within both summations, z is set to $z_i(t) = v_{zi}t$.

It is desirable to recast the time derivative in the first term of (35) using the relevant time scale ξ. For a given particle, z is determined by the integration over the δ function.

$$\begin{aligned} \xi &= ct - z = ct - v_{zi}t \\ \Rightarrow \frac{\partial\xi}{\partial t} &= c - v_{zi} \\ \Rightarrow \frac{\partial}{\partial t} &= (c - v_{zi})\frac{\partial}{\partial\xi} \end{aligned} \tag{36}$$

For the second term in (35), the $\hat{\mathbf{s}}$ component of the derivative is negligible in the quasi-static approximation. Hence (35) can be written,

$$\begin{aligned} 0 = \frac{\partial}{\partial\xi}\sum_i Q_i\left[1 - \beta_{zi}(\xi)\right]\delta\left(\mathbf{x}_\perp - \mathbf{x}_{\perp i}(\xi)\right) \\ + \boldsymbol{\nabla}_\perp\cdot\sum_i Q_i\frac{v_{\perp i}(\xi)}{c}\delta\left(\mathbf{x}_\perp - \mathbf{x}_{\perp i}(\xi)\right) \end{aligned} \tag{37}$$

(37) can be integrated over all x and y. The first term depends only on the longitudinal coordinate, and so the integration removes the δ function. The argument of the divergence in the second term is equal to 0 at the bounds of integration, and so the integral of this term is equal to 0. After integration, (37) becomes,

$$0 = \frac{\partial}{\partial\xi}\sum_i Q_i\left[1 - \beta_{zi}(\xi)\right] \tag{38}$$

Thus the quantity that is preserved as ξ is advanced is the effective charge,

$$q_i = Q_i\left[1 - \beta_{zi}(\xi)\right] \tag{39}$$

and not the absolute charge Q_i. The deposition is thus performed using the effective charge rather than the absolute charge,

$$\rho_p = \frac{1}{\text{volume}}\sum_i \frac{q_{pi}}{1 - \beta_{zi}(\xi)} \qquad \mathbf{J}_p = \frac{1}{\text{volume}}\sum_i \frac{q_{pi}\mathbf{v}_{pi}}{1 - \beta_{zi}(\xi)} \tag{40}$$

Two-dimensional wakefield sub-routine

The velocities of, and fields resulting from, plasma particles are interrelated; calculation of one requires knowledge of the other. The method by which the simulation algorithm advances the plasma particles in time requires some additional complexity to avoid the circularity of the trajectories and fields.

The simulation of the formation of the wakefield is carried out with time steps of size $\Delta\xi$. By choice, the velocity of the plasma particles is determined at whole-integer steps, and so the position of the plasma particles is determined at half-integer steps.

The objective is to determine the velocity $\mathbf{v}_p$ of a given plasma particle at step $m+1$ given the velocity of the plasma particle at step m. Advancing the velocity requires the fields at step $m+\frac{1}{2}$. Calculating the fields at $m+\frac{1}{2}$ requires ρ and $\mathbf{J}$ at step $m+\frac{1}{2}$. Depositing the plasma particles at step $m+\frac{1}{2}$ requires knowledge of the velocity of the plasma particles at step $m+\frac{1}{2}$. This is problematic, since the velocity of the plasma particles is only determined at whole-integer steps.

To avoid the circularity in advancing the velocity of the plasma particles, the charge deposition ρ_p and $\mathbf{J}_b$ are estimated at $m+\frac{1}{2}$ and iteratively corrected using the resulting value of $\mathbf{v}_p$ at $m+1$. The strategy is to first guess $\mathbf{J}_p$ and ρ_p at step $m+\frac{1}{2}$ so that $\mathbf{v}_p$ at $m+\frac{1}{2}$ is not needed. All fields at $m+\frac{1}{2}$ are then computed using the assumed plasma charge distribution and the beam deposition, which is fixed for a given value of s. The position and momentum of the plasma particles are advanced using the evolution equations, and the velocity $\mathbf{v}_p$ of the plasma particles at the subsequent time step $m+1$ is computed. The estimates of $\mathbf{J}$ and ρ at the intermediate step $m+\frac{1}{2}$ are then corrected based on the new calculated value of $\mathbf{v}_p$. This guess and correct algorithm can be repeated until the desired accuracy is obtained.

Implementation overview

A simplified schematic of QuickPIC algorithm is as follows:

1. At a given s, deposit beam particles in (x, y, ξ) space.
2. Call plasma sub-routine.
   (a) Initialize plasma particles at a value of ξ sufficiently ahead of the beam.
   (b) Push plasma particles forward in ξ.
      i. Calculate $\mathbf{v}_p$ from (32) and (33).
      ii. Deposit plasma particles by calculating ρ_p and $\mathbf{J}_p$ from (40).
      iii. Calculate the fields from (22), (23), and (24).
      iv. Calculate the derivatives necessary to evolve the position and momentum of the plasma particles using (32) and (34).
   (c) Repeat for each step in ξ.
3. After advancing the plasma particles in ξ, advance the beam in s.
4. Update the position and momentum of the beam particles and repeat.

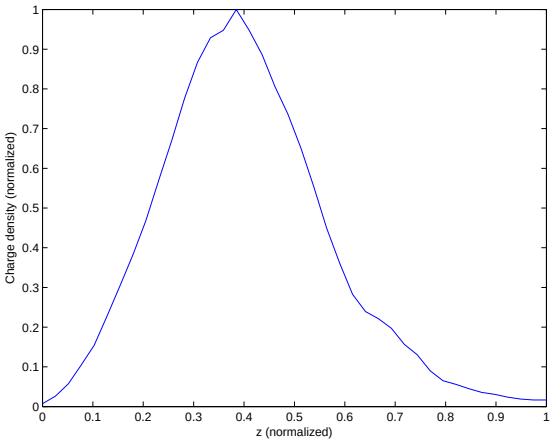

FIG. 11: Drive beam longitudinal density profile, in normalized units.

DATA

Simulation parameters

The simulations discussed in this paper use the QuickPIC algorithm to propagate an electron beam through one meter of plasma. The plasma results from self-ionization of a lithium vapor. The beam and plasma

Initial beam energy	$\gamma = 82192$
Transverse beam profile	Twiss parameters
Normalized emittances	$\epsilon_{Nx} = 100, \epsilon_{Ny} = 20$
Longitudinal profile	piecewise linear, figure 11
Longitudinal r.m.s. size	$\sigma_z = 31.8\,\mu$m
Beam charge	$q_{b,\mathrm{tot}} = 1.7 \times 10^{10} e$
Plasma charge density	$\rho_p = 2.7 \times 10^{17}$ cm^{-3}
Simulation step	$c\omega_p^{-1} = 10.23\ \mu$m

TABLE II: Parameter values used in simulations.

parameters are selected to model the conditions of the E-167 experiment. A summary of the simulation parameter values that follow is presented in table II.

The simulated drive beam is a pulse consisting of 1.7×10^{10} ultra-relativistic electrons. The beam is initialized to be precisely monoenergetic, with all beam electrons having relativistic boost $\gamma = 82192$. The normalized emittances, in units of mm·mrad, are 100 in the x direction and 20 in the y direction. The longitudinal profile of the beam is piecewise linear and somewhat Gaussian, as shown in figure 11. In physical units, the r.m.s. length of the drive bunch is 31.8 microns.

All longitudinal distances z are measured relative to the plane in which the beam enters the plasma, taken to be $z = 0$. The transverse beam profile is specified by the values of the Twiss parameters at $z = 0$. The density of the plasma is assumed to be sufficiently small that the drive beam focuses as if propagating through a vacuum.

The plasma is created by single ionization of lithium atoms upon impact of the drive beam. The simulations presented here do not include the effect of multiple ionization, which is expected to be small in this case due to the high secondary ionization potential of lithium. The density of the plasma is constant, 2.7×10^{17} cm^{-3}, from $z = 10$ cm onwards. Between $z = 0$ cm and $z = 10$ cm, the plasma density increases linearly from 0 to 2.7×10^{17} cm^{-3}.

The only parameters that are varied between simulations are the Twiss parameters at $z = 0$. By specifying the Twiss parameters, I vary the drive beam waist location from $z = 0$ to $z = 25$ cm in units of 5 cm. Unfortunately, it is not possible to simulate the case in which the waist is positioned at $z = 10$ cm due to numerical instability resulting from trapped particles.

Diagnostics

Unlike physical experiments, computer simulations allow exact diagnostics of beam and plasma parameters to be taken at regular intervals. The time interval of the simulation is equal to the inverse plasma frequency, $\frac{1}{\omega_p}$. The plasma frequency is evaluated in the constant density region of the plasma, $\omega_p \approx 2.931 \times 10^{13}$ s^{-1}. Since the beam is assumed to propagate at the speed of light, the distance traveled by the beam during each simulation time step is equal to the collisionless plasma skin depth, $\frac{c}{\omega_p} \approx 10.23$ microns.

Beam charge density is sampled every two time steps, and plasma charge density is sampled every ten time steps. This choice of timescales is chosen to be consistent with the quasi-static approximation, which assumes that the time scale for evolution of the wakefield is much less than that for the drive beam.

The ionization front is determined from the beam charge density as the plane of smallest z in which the beam charge density is non-zero. The evolution of the ionization front as a function of beam propagation distance is shown in figure 15.

Longitudinal electromagnetic fields in the plasma are measured every ten time steps in both the xz and yz planes. Although the length scales of the beam envelope in the two planes are different, the evolution of the fields is qualitatively very similar in the two transverse dimensions. Henceforth, I focus on the field in the xz plane.

From the electric field in the xz plane, I calculate the transformer ratio as a function of propagation distance, shown in figure 19. The transformer ratio is calculated based on the longitudinal profile of E_z in the $x = 0$ plane, and is equal to the ratio of the effective accelerating field to the maximum decelerating field. The maximum value of the profile of E_z along $x = 0$ within the first bucket is taken as the maximum decelerating field. Calculating the effective accelerating field is performed in several steps. The point at which E_z returns to 0 after achieving an initial maximum is first identified. The tangent to the profile of E_z along $x = 0$ is then estimated at this point. The effective accelerating field is taken as the intersect of this tangent with the near vertical step in E_z that occurs at the rear of the bucket.

Phase space data for the beam is output every two time steps, and contains x, y, z, p_x, p_y, and p_z. The data is recorded as continuous variables that must be binned and discretized on a grid. Figure 21 shows phase space data discretized with a mesh of 512 by 512 points. This sampling resolution is a compromise between resolution and computation time.

DISCUSSION

Energy

The dependence of the maximum and minimum particle energies on propagation distance is shown in figure 12. The maximum energy achieved appears to be greatest for beams focused near $z = 0$ and decreases with increasing focusing distance. The rate of energy gain of all beams is initially similar. However, energy gain produced by beams focused at larger z appears to be limited, whereas the rate of energy gain produced by the beam focused at $z = 0$ is constant until the disintegration of the beam. That shallowly focused beams achieve greater energy is not intuitive, since such beams tend to be more susceptible to instabilities that can detract from the energy available for acceleration.

Plotting the extrema of energy obtained over the full propagation distance of the beam in figure 13 confirms what is suggested by figure 12: shallowly focused drive beams accelerate the witness bunch to greater maximum energy. The maximum beam energy shows a clear downward trend with increasing waist distance, whereas the

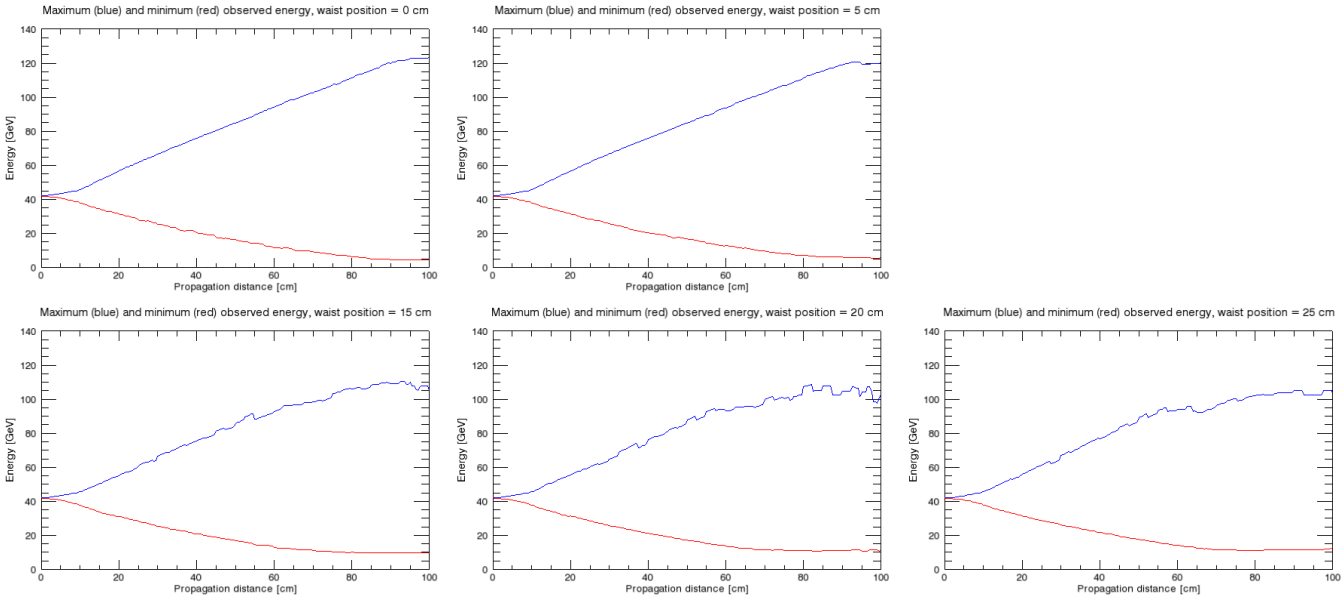

FIG. 12: Maximum and minimum energy of beam particles as a function of propagation distance. Beams focused near $z = 0$ achieve greater energy gain than those focused at larger z. Energy maxima change at a nearly constant rate in shallowly focused beams, whereas maxima appear to asymptote for more deeply focused beams. No beams appear to be limited by pump depletion.

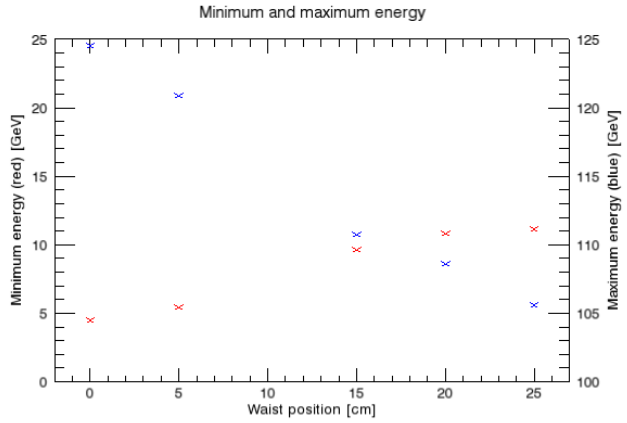

FIG. 13: Energy extrema of greatest magnitude achieved over total propagation distance. Energy maxima shows clear downward linear trend with increasing waist position. Energy minima display upwards linear trend with increasing waist position.

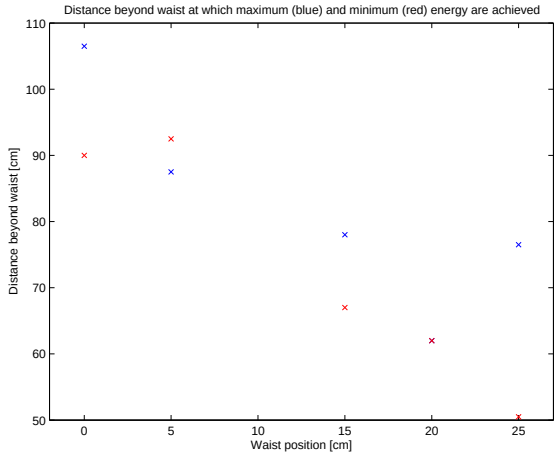

FIG. 14: Distance in z beyond waist location at which energy extrema plotted in figure 13 are achieved. Distance of extrema after beam waist generally decreases as waist location is increased. The decrease in distance at which extrema are achieved could be indicative of limitations due to poor ion channel formation by deeply focused beams with initially large transverse spot size.

minimum energy shows an increasing trend as waist distance is increased. Both of these dependences appear to be linear, although there is no a priori reason to expect this linearity.

The distance after the waist at which each extremum shown in figure 13 is achieved is plotted in figure 14. The location of these extrema relative to the waist location generally decreases for more deeply focused beams. This decrease is partly a simple consequence that, all other factors being equal, the distance to a extremum at constant location minus the distance to the beam waist decreases as the beam waist distance is increased. However, linear fits of the absolute maxima and minima locations, respectively, in figure 14 indicate that there is likely a waist-dependent component of the location of the extrema. The slopes of simple linear fits to the max-

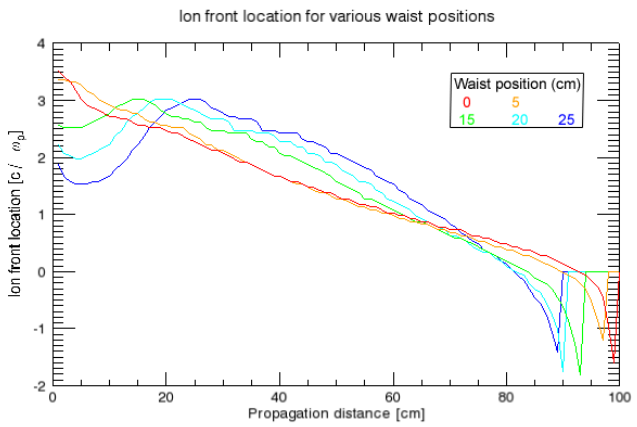

FIG. 15: Ionization front, defined as minimum ξ in beam comoving frame at which plasma charge density is nonzero. Order in which the ionization front location reduces to $\xi_{\rm ion} < -1$ (indicative of beam disintegration), shows that beams focused near $z = 0$ propagate further in the plasma than beams focused at larger z. Crossing of curves could indicate inefficient ion channel formation by deeply focused beams.

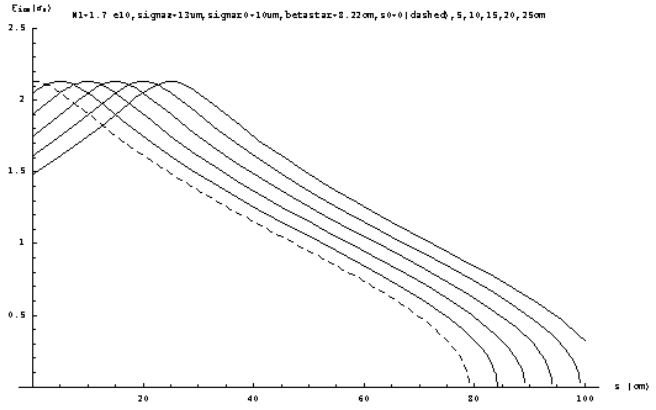

FIG. 16: Theoretical prediction for ionization front evolution as a function of propagation distance [12]. Simulations assume a symmetric beam and that the drive beam focuses as if in vacuum. Theory shows general agreement with simulation (figure 15), although theory does not predict crossing of ion front curves.

ima and minima locations have slopes of -1.3 ± 0.376 and -1.7 ± 0.282, respectively. If the location of extrema were independent of waist location, the relation between extrema and beam waist locations would be linear with a slope of -1.

Figure 12 indicates that in none of the simulations presented here does the beam energy reach 0. Hence the witness bunch energy gain does not appear to be limited by depletion of drive beam energy, a condition known as pump depletion.

The waist dependence of the energy extrema location and magnitude as well as the energy gain limitation could be do to variation in ion channel formation between beams focused at different locations. These possibilities are discussed below in relation to the ionization front.

Ionization front

The ionization front is measured in the comoving frame of the beam, in which the origin of coordinates is taken to be the center point of the initial head of the drive beam. The ionization front is defined as the smallest ξ at which the plasma charge density is nonzero. The ionization front as a function of propagation distance is shown in figure 15.

As shown in the figure, the ionization front is greatest in all cases at the location of the waist. This is consistent with (8) which predicts that the radial electric field governing ion channel formation is inversely proportional to beam transverse spot size. An ionization front at $\xi < -1$ is indicative of beam collapse. The order in which the beams in figure 15 collapse shows that beam propagation distance decreases with increasing waist distance.

The reduction in ionization front location that occurs at small z is not well understood. This reduction is not predicted by theory, and is not reproduced by figure 16. It is possible that the location of the ionization front is effected by the linear density ramp that occurs between $z = 0$ and $z = 10$ cm, although it is not clear why a less dense plasma would result in decreased ionization front location. More simulations with varying density ramps are necessary to further understand this behavior.

A theoretical prediction of ionization front evolution is shown in figure 16 [12]. This prediction is based on a symmetric beam with constant density, so the comparison to figure 15 is not exact. However, there is agreement with the general pattern of ionization front evolution: increase to a maximum at the beam waist, followed by a linear decrease, culminating in a sharp decrease as the beam collapses.

However, there are several notable differences between the theoretical and observed ionization front evolution. The ionization front curves of the three simulations focused after the plasma density ramp, with waist locations at $z = 15, 20$, and 25 cm respectively, achieve approximately the same maximum magnitude at their respective waists. These curves also intersect at approximately one point. The other two simulations which are focused within the z range of the plasma density ramp also have similar maximum magnitude and intersect at a single point. The maximum and intersection point of this second group is distinct from those of the group of simulations in which the beam is focused after the density ramp.

The apparent separation of the simulations into pre- and post-10 cm focusing groups may indicate the importance of the linear plasma density ramp between 0 and

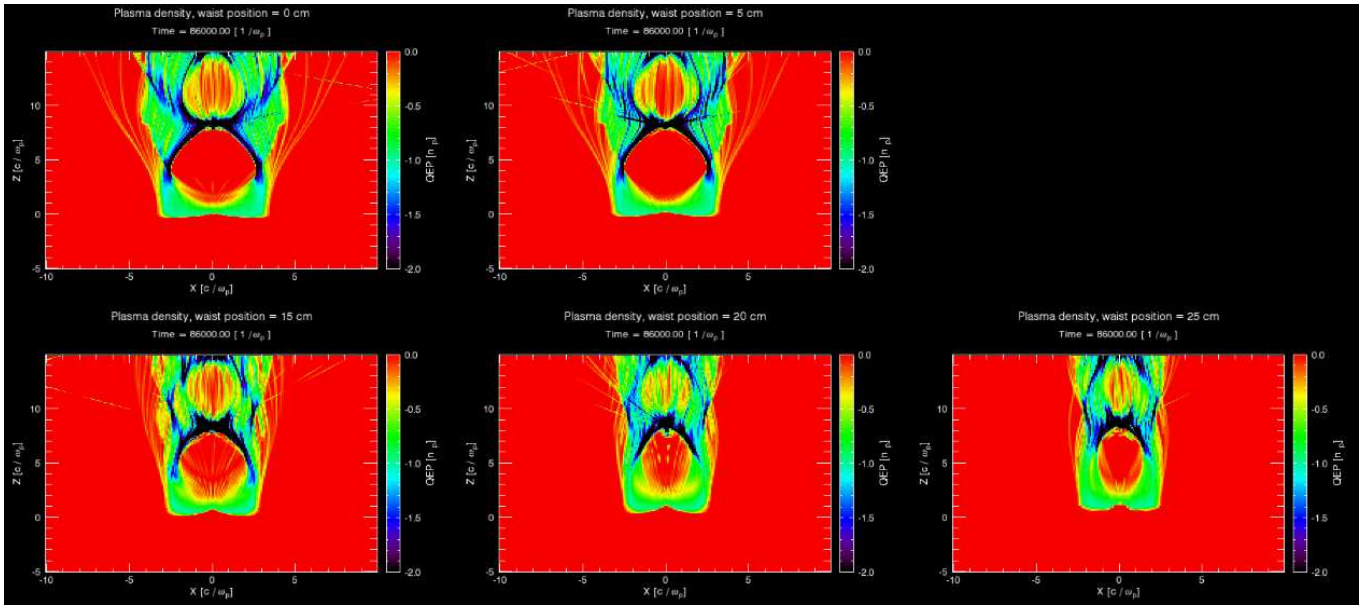

FIG. 17: Representative frame of beam charge density at $z \approx 86$ cm. The blown-out ion channel is smaller in the case of beams focused at large z. Ion channel formation my limit the energy obtained by deeply focused beams.

10 cm in determining the beam behavior at all further z. The effect of such plasma density variations has not previously been studied in depth, but initially we did not expect the density ramp to have a significant effect on drive beam propagation.

It is notable that the ionization front curves in figure 15 cross one another. This crossing indicates that beam structure degrades more rapidly for beams focused at larger z. A beam that is focused near $z = 0$ does not experience degradation comparable to that experienced by a beam focused at larger z even as the spot size of the beam focused at smaller z expands to be greater than that of the beam focused at larger z. Ion channel formation appears to be influenced by the history of the beam rather than simply the transverse spot size at a given point.

Beams that are focused at greater z have larger transverse spot sizes at $z = 0$. By (8), the transverse electric field which governs ion channel formation is initially less in such beams. Because of the inefficiency with which plasma electrons are expelled from the ion channel, the head of the drive beam could experience increased erosion early in the propagation of the beam. Head erosion would further decrease the transverse electric field, resulting in a positively reenforcing cycle that could explain the reduced propagation distance of beams focused at larger z.

Incomplete ionization of the ion channel by a weak transverse electric field would lead to a lower acceleration gradient as well as a smaller ion channel radius. It is possible that the efficiency of the wakefield structure could be reduced by the smaller radius of the ion channel or encroachment of the ionization front. Hence a self-reenforcing cycle of head erosion and incomplete ion channel formation could lead to limitations on the maximum beam energy.

Focusing of the drive beam by the plasma acceleration medium is another mechanism that could contribute to history dependence of the formation of the ion channel. Beams focused near $z = 0$ would be more able to achieve a pure ion channel at small z due to the smaller initial transverse spot size of such a beam. Once established, a pure ion channel could contributed to focusing of the beam due to strong radial electric fields. It would be difficult for a beam focused at larger z to establish comparable transverse fields that could lead to plasma focusing, since, as discussed above, such beams are likely more limited by head erosion. This plasma focusing would maintain the spot size of beam focused at small z to be less than that of a beam focused at larger z at a comparable distance relative to the respective beam waists.

A sample of the plasma charge density is shown in figure 17. This frame is taken from $z \approx 86$ cm, after considerable propagation distance, when differences in beam shape become more pronounced. The ionization channel of the beam focused at $z = 25$ cm is narrower and shorter than that of the beams focused at smaller z. More deeply focused beams also show evidence of incomplete ionization of the ion column, which would reduce the strength of the resulting accelerating field.

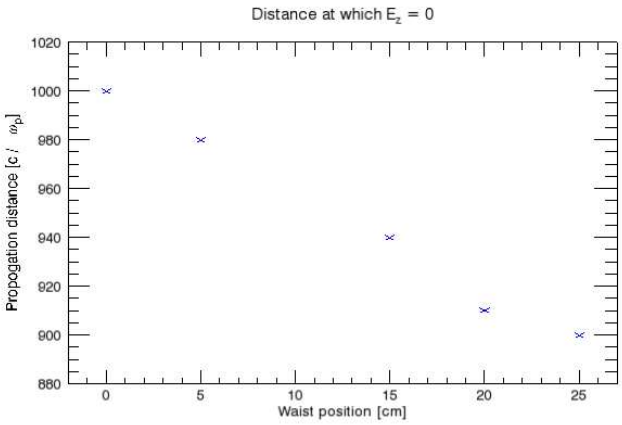

FIG. 18: Location in z at which E_z in the comoving frame of the beam becomes 0. The electric field confirms the previous assertion that beams focused near $z = 0$ propagate farther in the plasma than those focused at larger z.

Electric field

Observations of the electric fields within the plasma support conclusions that have already been drawn from other parameters. The location in z at which the longitudinal electric field becomes identically equal to 0 for a given simulation is a measure of the maximum distance to which the drive beam propagates before disintegration. As shown in figure 18, the beam focused at smallest z propagates furthest into the plasma, and propagation distance decreases as focusing distance is increased. The relationship between beam waist location and propagation distance appears to be linear, although there is not yet a clear theoretical motivation for this linearity.

The transformer ratio as a function of propagation distance is plotted in figure 19. The transformer ratio for beams focused at smaller z is more constant than the transformer ratio of beams focused at larger z. The accelerating and decelerating fields, as indicated by the slopes the lines of maximum and minimum energy in figure 12, do not appear initially to be significantly greater in the case of focusing at small z as opposed to large z. Rather, these fields are more constant over a larger range of z in the case of a shallowly focused beam. Constant accelerating and decelerating fields is consistent with a more uniform transformer ratio.

Relation to E-167 experiment

Because of the limitations of experimental diagnostics, physical observations can potentially differ from simulation results. In the case of the E-167 experiment, the energy diagnostics used have a minimum sensitivity, which effects the way in which the energies plotted in figure 12 would be observed. The transverse size of the observable window is larger in the E-167 experiments than in the simulations presented here, and so particles that are not included in these simulations may be imaged by the E-167 experimental apparatus.

The energy diagnostics used in the E-167 experiment require about 5×10^6 electrons per GeV at a given energy in order to produce an observable signal. The maximum energy at which the simulation results achieve this energy is shown in figure 20. Beams focused at smaller z produce the largest energy gains. However, in the experimental case, the maximum observable energy is about 90 GeV rather than 110 GeV. Observing particles with 90 GeV of energy would still indicate an extremely large acceleration gradient of about 50 GeV per meter.

It appears that the beam focused at 25 cm may achieve greater maximum observable energy than beams with waists at 15 or 20 cm. The beam focused at 25 cm may be more mono-energetic at high energy due to the fact that the limit on the maximum energy achievable by the beam focused at 25 cm is less than that of the beams focused at 15 and 20 cm, respectively. Hence the beam focused at 25 cm appears experimentally to achieve higher energy due to a lack of particles at higher energies in unobservably small quantities.

No simulation energy spectrums, shown in figure 21, evidence a tail of low energy particles like that shown in the experimental data, figure 9. All simulations appear to have a flat-bottomed energy spectrum, with the minimum energy increasing as waist distance is increased.

The plot of the beam energies provides further support for several previous assertions. That the minimum energy observed in each simulation is nonzero is indicative that acceleration does not appear to be limited by pump depletion. The beams shown in figure 21 are beginning to degrade due to instabilities. These instabilities are terminal and lead to the eventual disintegration of the beam. The severity with which the beams are effected by instabilities increases with focusing distance, indicating that shallowly focused beams propagate farther through the plasma.

The simulations presented here suggest that the tail of low energy particles observed experimentally is not due to variation of drive beam waist location. These low energy particles are also not likely due to pump depletion, as the drive beam does not appear to be depleted of energy upon disintegration of the beam.

A remaining possibility for the origin of experimentally observed low energy particles is self-trapping by the wakefield structure. The simulation box used in these simulations is smaller than the experimentally observable transverse window. The number of particles in the simulation box decreases as the beam propagates in all simulations, as shown in figure 22. It is possible that particles lost from the simulation remain within the larger experimental window. These particles that have left the simulation window will not be accelerated as effectively

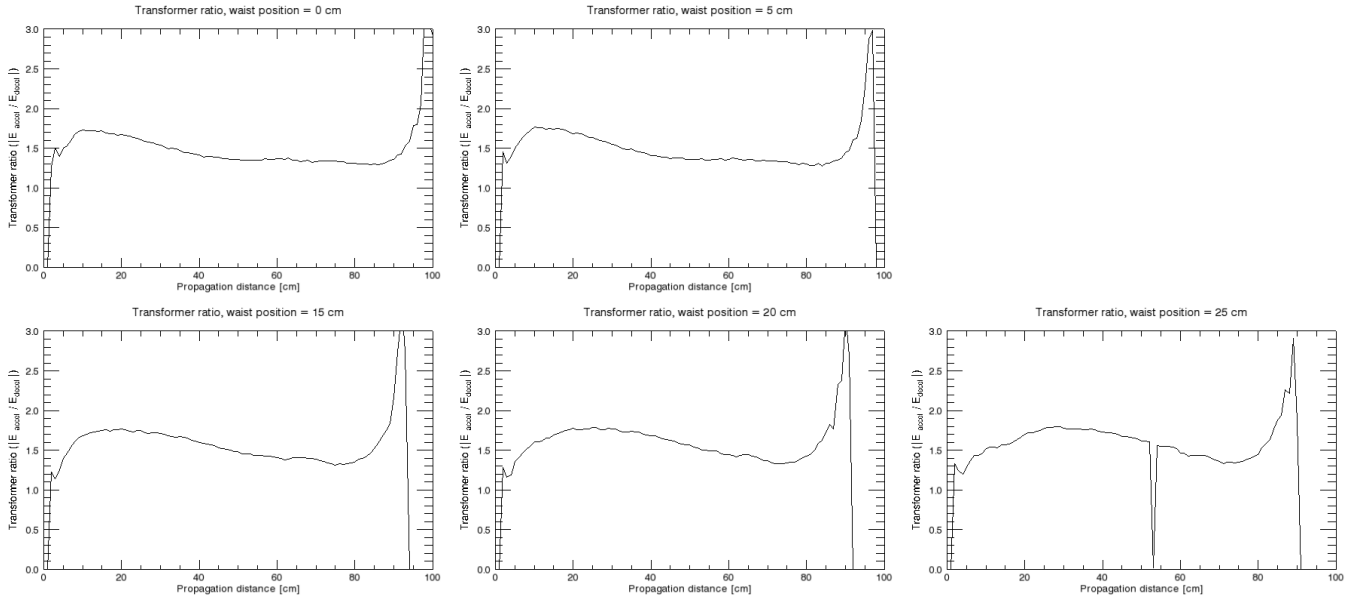

FIG. 19: Transformer ratio, defined as the ratio of the effective accelerating field to the maximum decelerating field. All beams show maximum transformer ratio near waist, consistent with a larger accelerating field due to a smaller transverse spot size. Transformer ration of beams focused near $z = 0$ are relatively constant, consistent with nearly constant change in energy maxima. Spike in curve for waist at 25 cm is due to computational algorithm and is not a physical effect.

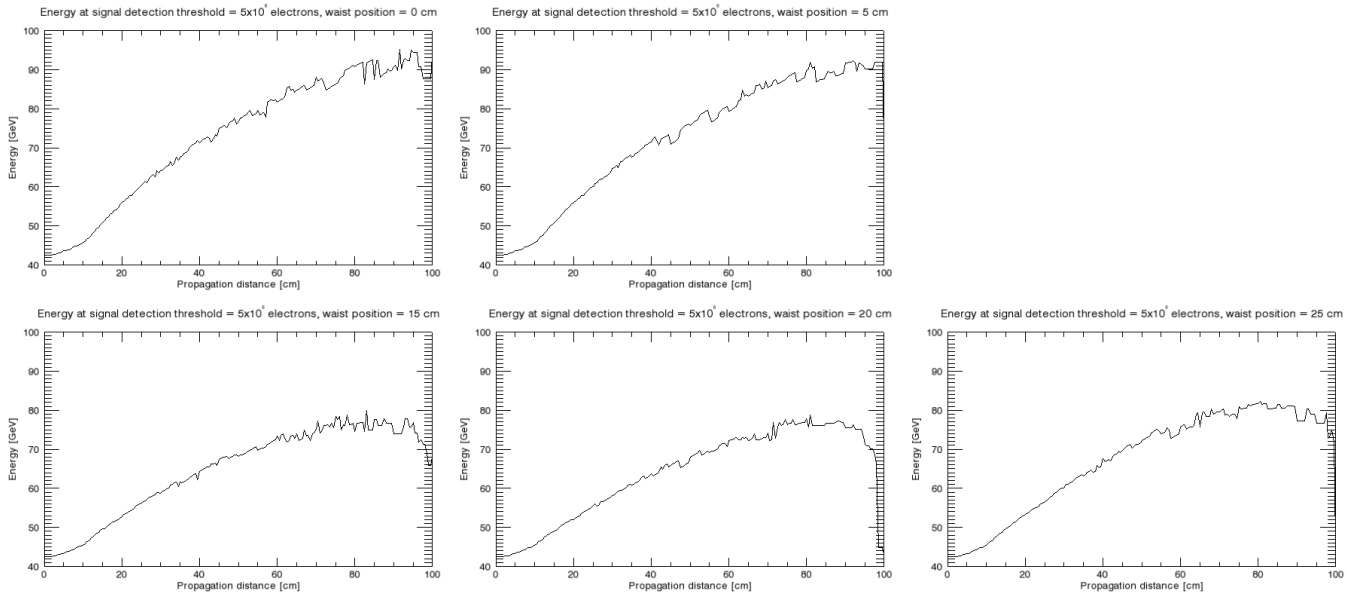

FIG. 20: Maximum energy observable by E-167 experiment apparatus. Results are similar to simulation, figure 12. Maximum observable energy is smaller and change is not as constant for beams focused at small z; nevertheless, the energy of some particles is more than doubled.

once ejected from the wakefield structure. Hence these particles, if imaged by the experimental energy diagnostic, could produce a tail like that shown in figure 9. These predictions may be better confirmed as the QuickPIC simulation algorithm is improved to better model self-trapping of plasma particles.

CONCLUSION

In this paper, I present five simulations in which I vary the waist location of a beam of ultra-relativistic electrons propagating through one meter of self-ionized lithium plasma. The simulation parameters are chosen to emulate the recent SLAC E-167 experiments, with the

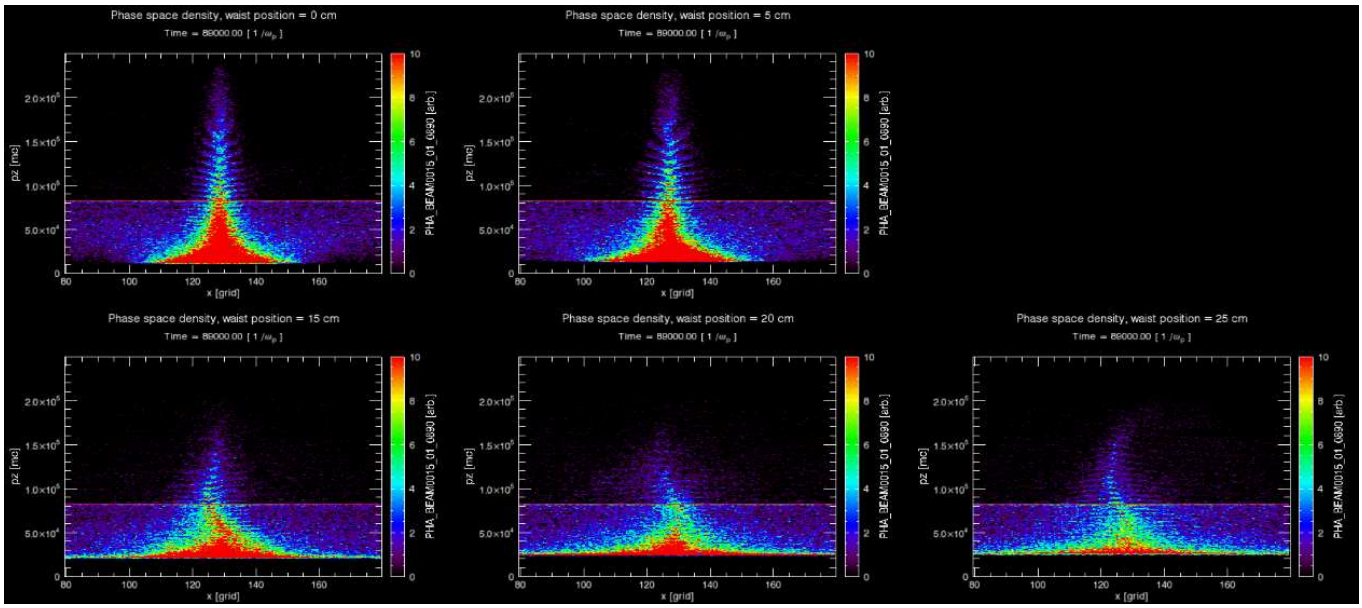

FIG. 21: Phase space plot of pz verses x from simulations. Vertical scale in these plots is proportional to vertical scale of experimentally observed energy spectrum, figure 9. None of the waist locations tested reproduced the monotonic tail of very low energy particles shown present in the experimental data.

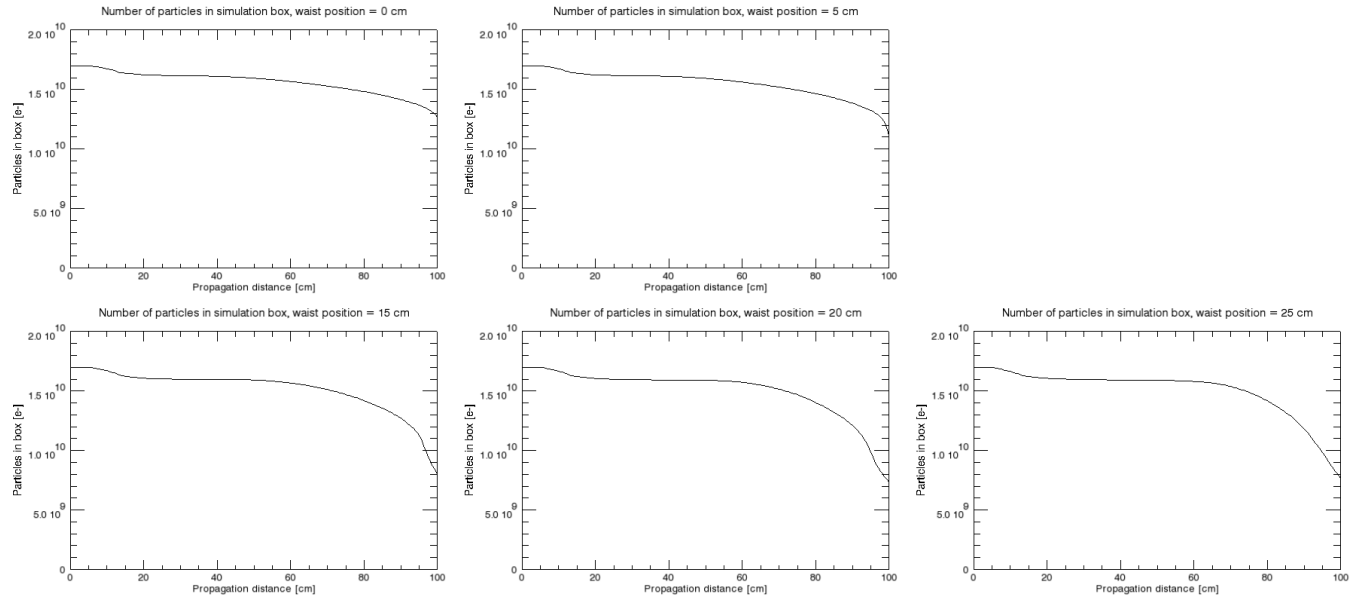

FIG. 22: Particles in simulation box as a function of propagation distance. Particles lost from simulation box could potentially be imaged by experimental apparatus. These ejected particles would be at lower energy than other beam particles and could possibly form the tail of low energy particles observed experimentally.

objective of reproducing the tail of low energy particles observed by these experiments.

I find that focusing the drive beam near $z = 0$ results in greater maximum energy achieved by the witness bunch compared to focusing at larger z. Shallowly focused beams also propagate further through the plasma acceleration medium than those focused more deeply.

Maximum energy gain and propagation distance could be dependent on the effect of transverse beam spot size on ion channel formation. Beams focused at larger z could experience a self-reenforcing cycle of head erosion that limits beam propagation distance and ion channel formation. Plasma focusing may maintain the transverse spot size of beams focused at smaller z to be less than that of beams focused at larger z at a comparable distance from the beam waist.

None of the simulations presented here show evidence of a tail of particles at very low energy, as observed in the E-167 experiments, nor do any simulations show signs of pump depletion. These negative results, and evidence of loss of simulation particles, raise the possibility that low energy particles experimentally observed could be electrons trapped within the wakefield structure.

I would like to thank Professor W. B. Mori and Miaomiao Zhou for their guidance in preparing this research. I would also like to thank Françoise Quéval and the National Science Foundation Research Experiences for Undergraduates program for their generosity and support.

* adriand@berkeley.edu
† Department of Physics, University of California, Berkeley

[1] J. Dawson, Scientific American pp. 54–61 (1989).
[2] C. Joshi, Scientific American pp. 41–47 (2006).
[3] C. Joshi, Physics Today pp. 47–53 (2003).
[4] F. J. Decker and et. al. (2005), e-167 Proposal.
[5] W. Lu, C. Huang, M. Zhou, W. B. Mori, and T. Katsouleas, Physical Review Letters **96**, 165002 (2006).
[6] K. Fournier, *Recent Progress on Laser-Driven X-Ray Sources*, Presentation to members of the UCLA EE department (2006).
[7] K. G. Steffen, *High Energy Beam Optics*, Interscience Monographs and Texts in Physics and Astronomy (Wiley & Sons, 1965).
[8] C. Huang, V. K. Decyk, C. Ren, M. Zhou, W. Lu, W. B. Mori, J. H. Cooley, T. M. Antonsen, and T. Katsouleas, Journal of Computational Physics (2006).
[9] E167 Collaboration, Preliminary data from E167, obtained from personal communication with M. Zhou.
[10] C. Joshi and et. al., Physics of Plasmas **9**, 1845 (2002).
[11] A. A. Geraci and D. H. Whittum, Physics of Plasmas **7**, 3431 (2000).
[12] M. Zhou, Master's thesis, University of California, Los Angeles (2005).
[13] P. Michel and et. al. (2006), Physical Review Letters, E.
[14] D. H. Whittum, W. M. Sharp, S. S. Yu, M. Lampe, and G. Joyce, Phyical Review Letters **67**, 991 (1991).
[15] M. J. Hogan, C. D. Barnes, C. E. Clayton, and et al., Physical Review Letters **95**, 054802 (2005).
[16] J. B. Rosenzweig, A. Murokh, and A. Tremaine, AIP Conference Proceedings **472**, 38 (1999).